

but

$$\psi(t+T) = \exp(-i \frac{T}{2} V) \exp(-iT H) \exp(-i \frac{T}{2} V) \psi(t) + O(T^3)$$

2.D Interferometric photo emission

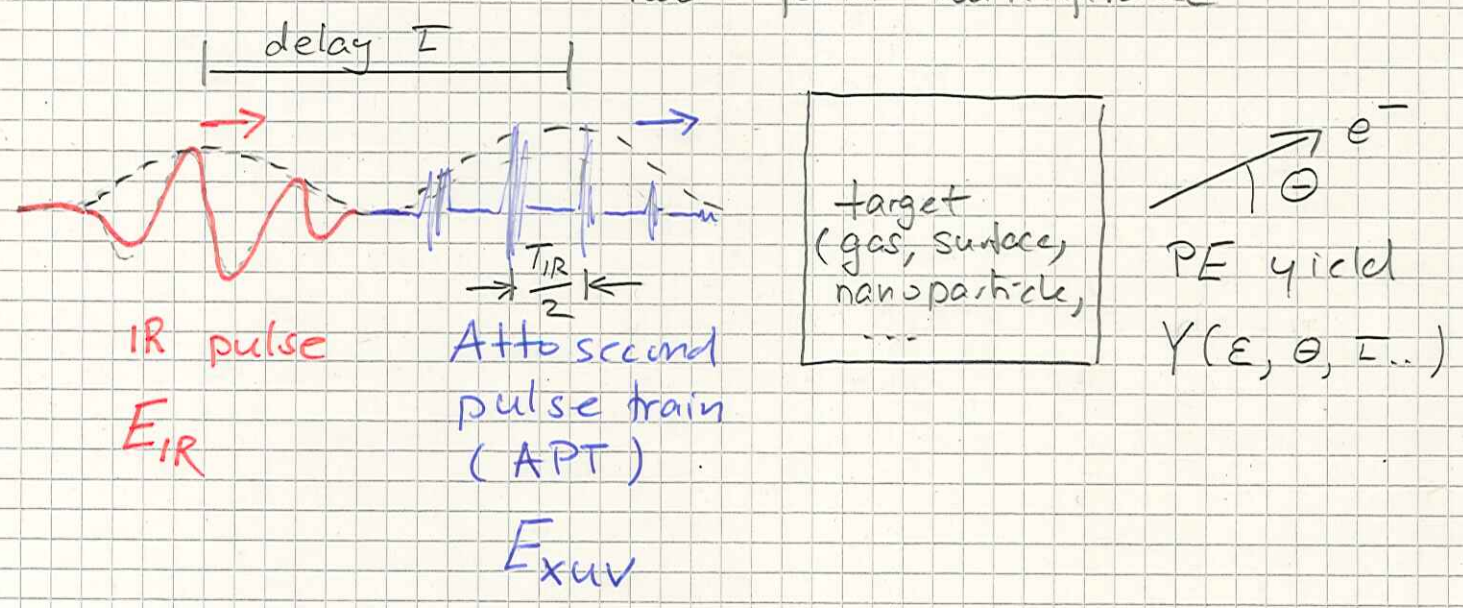
$\hat{=}$ RABITT spectroscopy

(reconstruction of attosecond beating by interference of two-photon transitions)

↑
or more (\rightarrow multiple sidebands)

• Basic idea for single side bands:

two-path interference



$$E_{xuv} = -\frac{\partial}{\partial t} A_{xuv}(t)$$

$$A_{xuv} = \sum_n A_{xuv}^{2n+1}(t) \quad \text{Supposition of high harmonics}$$

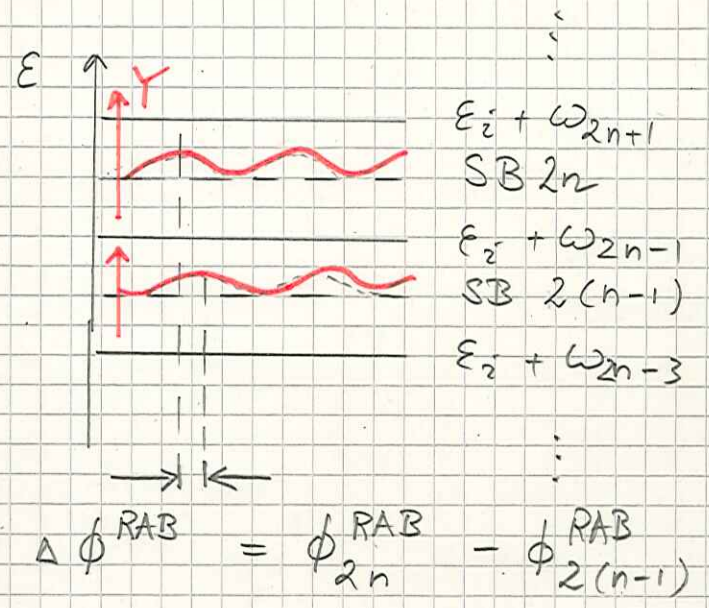
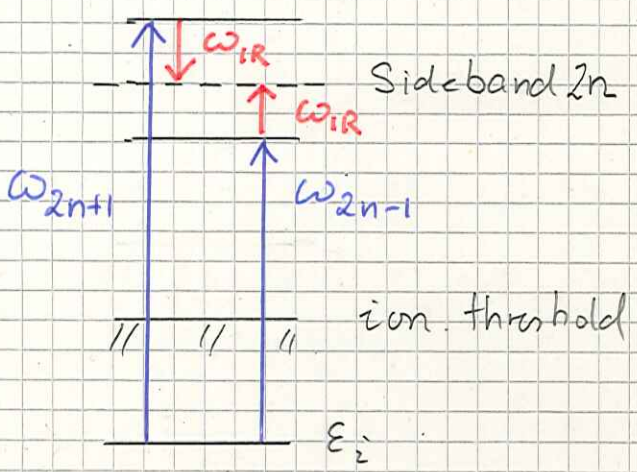
$$A_{xuv}^{2n+1} = a_{xuv}^{2n+1} \rho_{xuv}^{2n+1}(t) e^{i(\varphi_{2n+1} - \omega_{2n+1} t + \frac{H_H}{2n+1})}$$

\downarrow
 $(2n+1) \omega_{IR}$

$a_{xuv}^{2n+1} \in \mathbb{R}$: harmonic amplitude

f_{xuv}^{2n+1} : harmonic envelope, e.g. $\sim e^{-\alpha_{2n+1} t^2}$

ϕ_{2n+1}^{HH} : harmonic phase



PE yield near SB $2n$

$$Y \sim Y_0 + Y_1 \cos(2\omega_{iR} t + \phi_{2n}^{RAB})$$

RABITT phase

$$\phi_{2n}^{RAB} = \phi_{2n-1}^+ - \phi_{2n+1}^- + \underbrace{\phi_{2n+1}^{HH} - \phi_{2n-1}^{HH}}_{\text{usually unknown}}$$

D.1 Gaseous atomic targets

Example : Interferometric photoemission from the 2s & 2p sub shells of Ne.

- Isinger et al., Science 358, 893 (2017) (Fig. 2, Figs. 3A, C)

Photoionization in the time and frequency domain *Science* 358, 893–896 (2017)

M. Isinger,^{1*} R. J. Squibb,² D. Busto,¹ S. Zhong,¹ A. Harth,¹ D. Kroon,¹ S. Nandi,¹ C. L. Arnold,¹ M. Miranda,¹ J. M. Dahlström,^{1,3} E. Lindroth,³ R. Feifel,² M. Gisselbrecht,¹ A. L’Huillier¹

We determine photoionization time delays in neon atoms over a 40–electron volt energy range with an interferometric technique combining high temporal and spectral resolution. We spectrally disentangle direct ionization from ionization with shake-up, in which a second electron is left in an excited state, and obtain excellent agreement with theoretical calculations, thereby solving a puzzle raised by 7-year-old measurements.

Fig. 1. Photoionization time delays in neon.

(A) Time delay differences [$\tau_A(2s) - \tau_A(2p)$] in neon as a function of photon energy for the two spectra shown in (B) (yellow and red dots). Theoretical calculations within many-body perturbation theory (black solid line) agree very well with the experimental data. Also shown is the streaking experiment from (7) (square), as well as the measured time delay differences [$\tau_A(su) - \tau_A(2p)$] between shake-up and 2p ionization (diamonds). (B) Photon spectra used in the measurement. High-order harmonics are generated in neon gas and filtered with a combination of 200-nm-thick Al and Zr filters (yellow spectrum) and with two Zr filters (red spectrum). The dashed lines illustrate the transmission curves of the two combinations of filters (40).

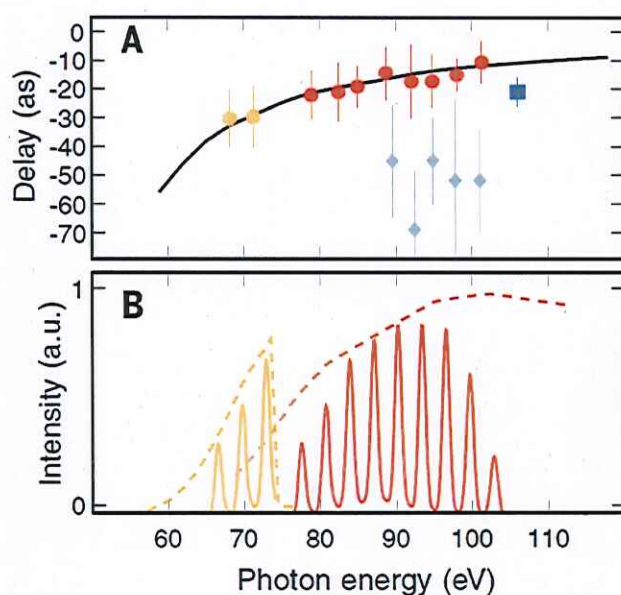
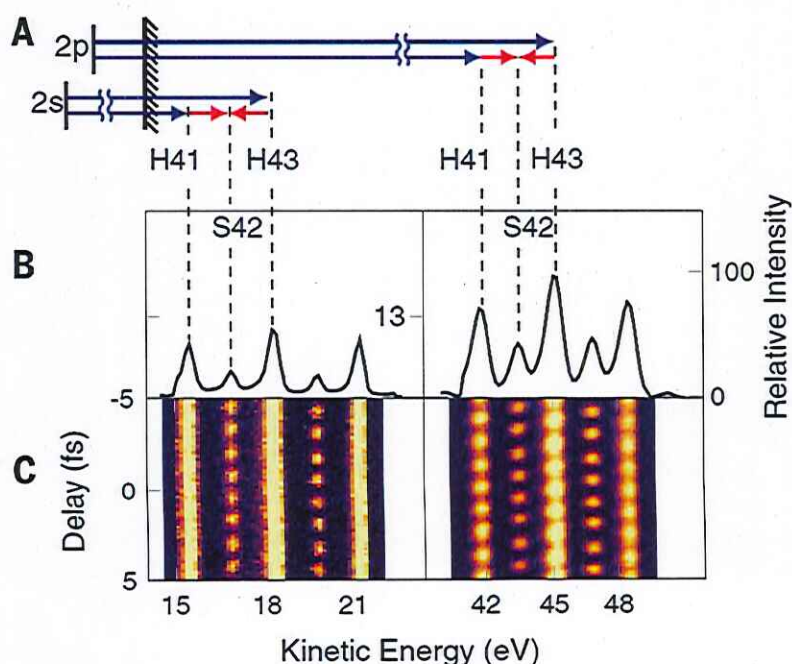


Fig. 2. Principle of the interferometric technique.

(A) Kinetic energy diagram for ionization from the 2s and 2p subshells using XUV (blue arrows) and IR (red arrows) radiation. (B) Time-averaged photoelectron spectrum obtained with Al-Zr-filtered harmonics. For both the 2s and 2p subshells, ionization results in three peaks due to absorption of harmonics (H41, H43, and H45) and two sideband peaks (S42 and S44) reachable by two-color two-photon transitions. (C) Photoelectron spectrum as a function of delay between the XUV pulse train and the IR field. The sideband amplitudes strongly oscillate as a function of delay.

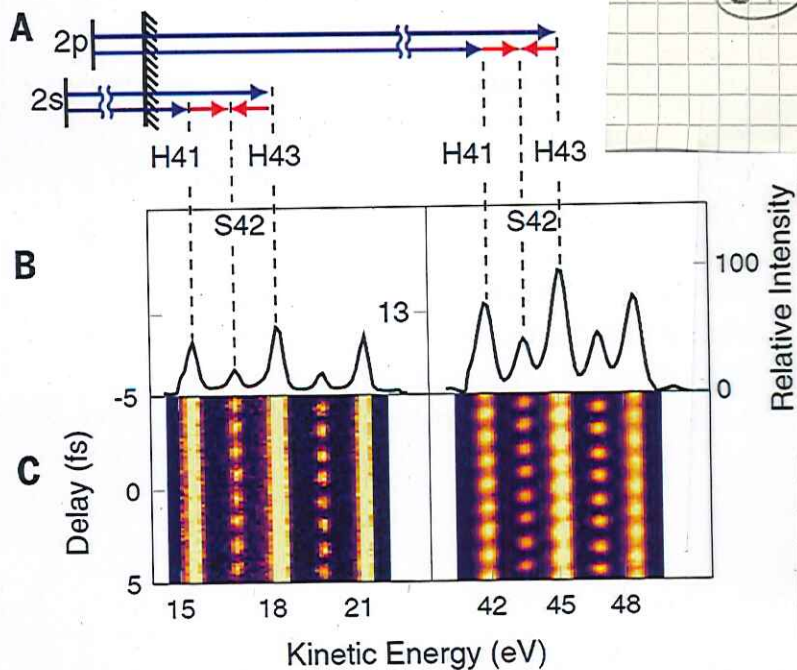


Principle of the interferometric technique.

(A) Kinetic energy diagram for ionization from the 2s and 2p subshells using XUV (blue arrows) and IR (red arrows) radiation.

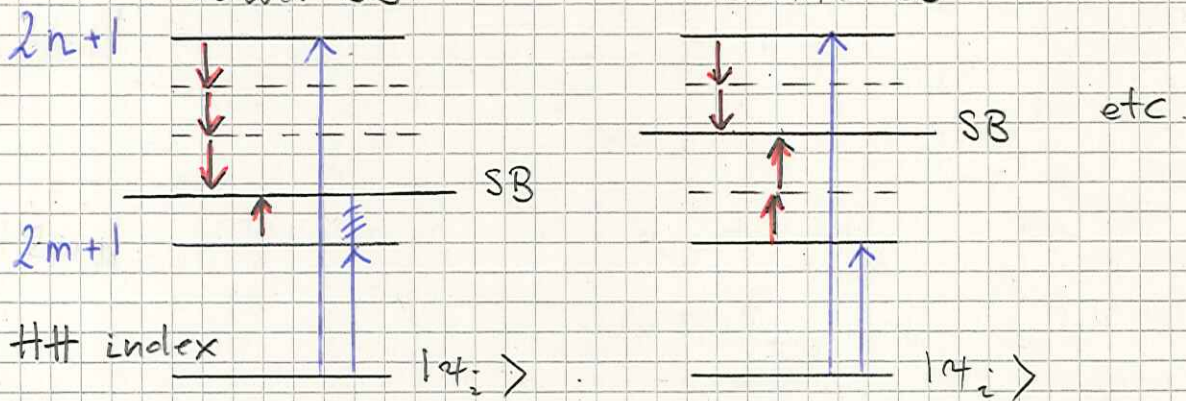
(B) Time-averaged photoelectron spectrum obtained with Al-Zr-filtered harmonics. For both the 2s and 2p subshells, ionization results in three peaks due to absorption of harmonics (H41, H43, and H45) and two sideband peaks (S42 and S44) reachable by two-color two-photon transitions.

(C) Photoelectron spectrum as a function of delay between the XUV pulse train and the IR field. The sideband amplitudes strongly oscillate as a function of delay.



Multi sidebanded RABBITT spectra

IR-assisted XUV photoemission spectra may have observable sidebands that involve more than two IR photons, especially at higher IR intensities, for example 4 IR photon SBs:



In addition, the two interfering channels can involve any pair of harmonics in the attosecond pulse train, i.e., $m \neq n$ is possible.

Fig. 3. Energy-resolved interferometric technique and identification of shake-up process.

(A) Kinetic energy diagram for 2s and 2p ionization accompanied by 2p \rightarrow 3p excitation (shake-up). The difference in threshold energy for these two processes is approximately 7.4 eV (11, 17). (B) Photoelectron spectra obtained with XUV only (blue) and XUV + IR (red). The electron peak due to shake-up induced by absorption of H61 partly overlaps with S56 from 2s ionization. The shoulder on the S56 (red spectrum) can be attributed to one-photon induced shake-up. (C) Energy-resolved intensity and phase of the 2ω oscillation, obtained by Fourier transforming the signal. The shake-up harmonic oscillates out of phase with the sideband, causing a sudden drop in the energy-resolved phase. The sideband originating from the shake-up state can be distinguished on the right side, allowing for a separate analysis of its time delay.

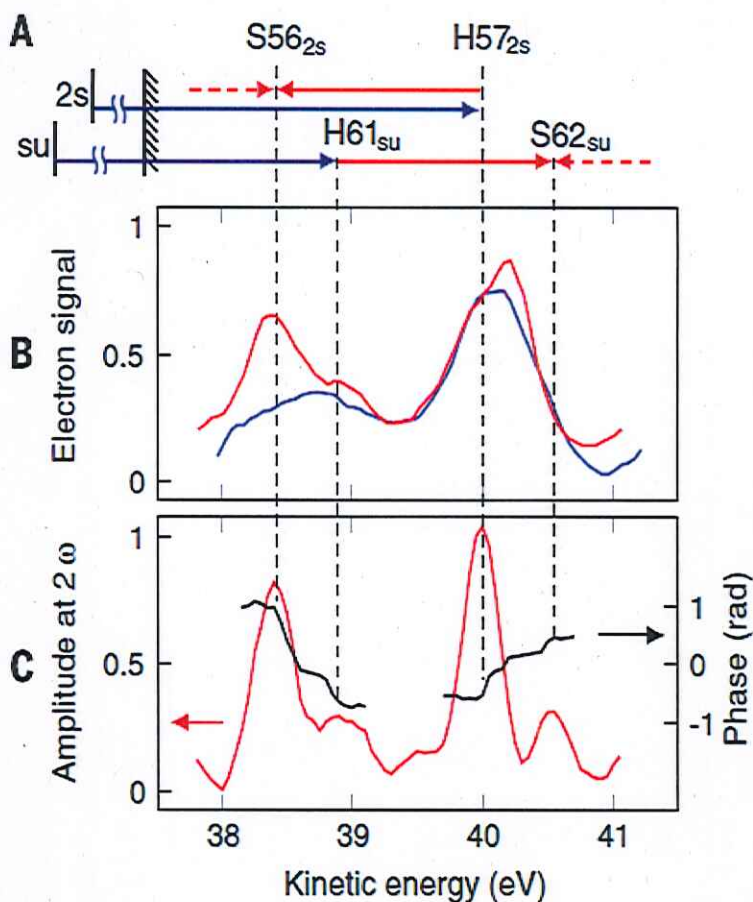
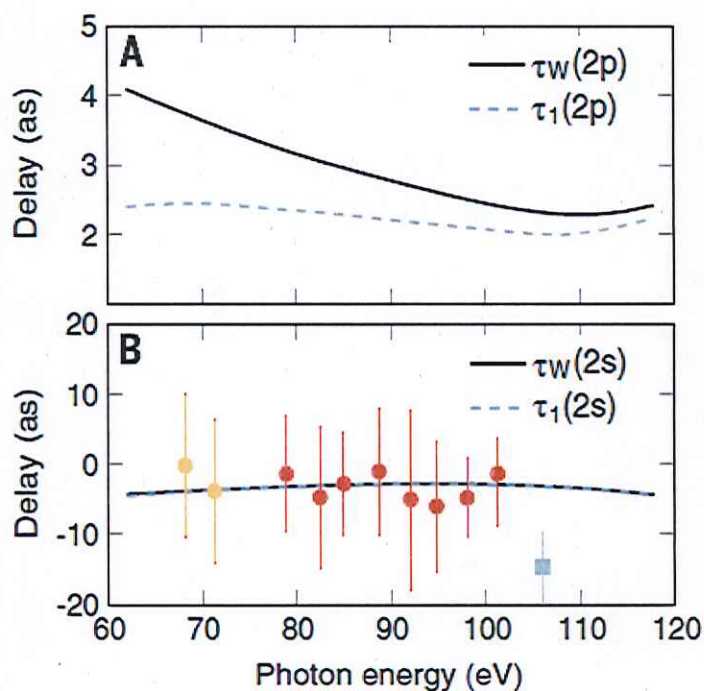


Fig. 4. Absolute photoionization time delays.

(A) Calculated Wigner delay $\tau_w(2p)$ along the direction of the light polarization as a function of the photon energy (black solid line). The dashed line indicates the angle-averaged one-photon ionization time delay accessible in the experiment. The difference between the two quantities is less than two attoseconds over the whole energy range. (B) Same as in (A) for 2s ionization. The difference between $\tau_w(2s)$ and $\tau_1(2s)$ is not visible. The experimental data [this work, yellow and red dots, and (7), square] is transformed to $\tau_1(2s)$ by subtraction of the analytical $\tau_{cc}(2s)$ and simulated $\tau_1(2p)$.



To develop a formalism that accounts for all XUV + IR two-channel interferences, let's start with the transition amplitude for the emission of a photon electron with momentum \vec{k} from the initial state $|i\rangle$,

$$T_{\vec{k},i}(T) = -i \int dt \langle \psi_{\vec{k}}(t) | z \cdot E_{XUV}(t+T) | \psi_i(t) \rangle,$$

$$\psi_{\vec{k}}(\vec{r}, t) \approx \psi_{\vec{k}}^V(\vec{r}, t) = (2\pi)^{-3/2} e^{i[\vec{k} + \vec{A}_{IR}(t)] \cdot \vec{r} - i\phi_{\vec{k}}^V(t)}$$

$-iE_{\vec{k}}t$

with the Volkov phase

$$\phi_{\vec{k}}^V(t) = \frac{1}{2} \int_t^\infty dt' [2\vec{k} \cdot \vec{A}_{IR}(t') + A_{IR}^2(t')]$$

The photoemission probability out of $|i\rangle$ is then given by

$$P(\vec{k}, T) = |T_{\vec{k},i}(T)|^2$$

$$= \left| \int dt E_{XUV}(t+T) d_{\vec{k},i} e^{i[E_{\vec{k}} - \epsilon_i]t + i\phi_{\vec{k}}^V(t)} \right|^2$$

(*)

where we consider just one initial state and

where

$$d_{\vec{k},i}(t) = (2\pi)^{-3/2} \int d^3r e^{-i\vec{p}(t) \cdot \vec{r}} \psi_i(\vec{r})$$

$$\vec{p}(t) = \vec{k} + \vec{A}_{IR}(t) \quad (\text{canonical momentum})$$

$$\psi_i(t) = \psi_i(\vec{r}) e^{-i\epsilon_i t}$$

✓ Atto second pulse train (linear polarization)

$$E_{xuv}(t) = \sum_j E_{xuv,j}(t) \exp(-i\omega_j t + i\phi_j^{xuv})$$

$$\begin{array}{ccc} E_{xuv,j} & f_{xuv}(t) & \text{HH phase} \\ \uparrow & & \uparrow \\ \text{HH amplitude} & & \end{array}$$

where

$$|f_{xuv}(t)| \leq 1 \quad \text{HH profiles, assumed equal}$$

$$\text{e.g. } f_{xuv}(t) = \exp\left\{-2\ln 2 \left(\frac{t}{T_{xuv}}\right)^2\right\}$$

$$\omega_j = j \omega_{IR} \quad (\text{usually } j \text{ is an odd integer})$$

✓ Bessel expansion of Volkov phase factor

$$e^{-i\phi_{\vec{R}}^V(t)} = \sum_n e^{in\omega_{IR}t} (-1)^n J_{|n|} \left[\vec{R} \cdot \vec{E}_{IR,0}(t) / \omega_{IR}^2 \right]$$

where

$$\vec{E}_{IR}(t) = \vec{E}_{IR,0}(t) \cos(\omega_{IR}t)$$

$$\vec{E}_{IR,0}(t) = \vec{E}_{IR,0} f_{IR}(t)$$

$$f_{IR}(t) \stackrel{\text{e.g.}}{=} \exp\left\{-2\ln 2 \left(t/T_{IR}\right)^2\right\}$$

In slowly varying envelope approximation

$$\vec{A}_{IR}(t) = - \frac{\vec{E}_{IR,0}(t)}{\omega_{IR}} \sin(\omega_{IR}t)$$

Assuming $\vec{E}_{IR} \uparrow \hat{e}_z$

$$\vec{R} \cdot \vec{E}_{IR,0}(t) = R E_{IR,0}(t) \cos\theta$$

Will assume sufficiently weak IR fields and PE energies so that

$$J_n(x) \approx \frac{1}{n!} \left(\frac{x}{2}\right)^n \text{ holds (for transparency).}$$

In practice, this assumption needs to be checked (numerically) and, if needed, more expansion terms need to be added until convergence is achieved. Then:

$$e^{+i\phi_{\vec{R}}^V(t)} = \sum_n \frac{(-1)^{|n|}}{2^{|n|} |n|!} e^{-in\omega_{IR}t} (\vec{R} E_{IR,0}(t) \cos\theta)^{|n|}$$

Pulling time-independent factors out of $\int dt$ we now have

$$\begin{aligned}
P(\vec{R}, I) = & \left| \sum_j E_{xuv,j} e^{i[\phi_j^{xuv} - \omega_j I]} \right. \\
& \times \sum_n \frac{(-1)^{|n|}}{2^{|n|} |n|!} (\vec{R} E_{IR,0} \cos\theta)^{|n|} \\
& \times \int dt f_{xuv}(t+I) [f_{IR}(t)]^{|n|} \left| \frac{d_{\vec{R}i}}{Ri} (t) \right| e^{i\phi_j(t)} \\
& \times e^{-i \left[\underbrace{E_i + (j+\omega)\omega_{IR} - E_{\vec{R}}}_{\approx \text{energy conservation } (=0)} \right] t} \Big|^2
\end{aligned}$$

small $\left| \frac{d}{dt} f_{xuv/IR} \right|$

where

$n \begin{cases} < \\ > \end{cases} 0$ corresponds to $\begin{cases} \text{emission} \\ \text{absorption} \end{cases}$ of IR photons.

and where we introduced to dipole phase ϵ_j , assuming it does not change over the spectral width of each $\#j$:

$$d_{\vec{R},i} = |d_{\vec{R},i}| e^{i\epsilon_j}$$

2 path interference

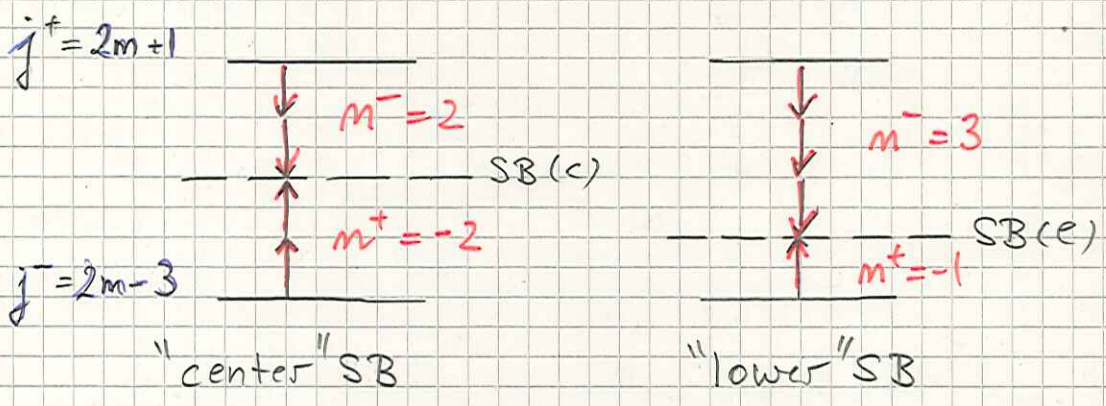
- pick two terms in \sum_j : $j^+ > j^-$
- pick two terms in \sum_n : n^+, n^-

make sure to arrive at the same final kin. energy $E_{\vec{R}}$

$$E_i + (j^- + n^+) \omega_{IR} \stackrel{!}{=} E_i + (j^+ + n^-) \omega_{IR}$$

$$\text{or } j^- + n^+ = j^+ + n^-$$

Sidg band intensities by example



Assume: $E_{xuv,j^+} = E_{xuv,j^-} = E_{xuv}$

Note: We are resonant ("m shell"), so the last exponential on p. 57 is = 1.

$$P(\vec{R}, L) = | (j^+, n^-) + (j^-, n^+) |^2$$

$$= \underbrace{|(j^+, n^-)|^2 + |(j^-, n^+)|^2}_{\text{incoherent terms}} + \underbrace{2 \operatorname{Re} \{ (j^+, n^-) (j^-, n^+)^* \}}_{\text{interference term}}$$

center SB : $n^- = -n^+ = 2$, assume $f_{xuv}(\pm) = \delta(\pm)$

$$P^{(c)}(\vec{R}, L) \approx \frac{E_{xuv}^2}{64} \left[E_{IR,0} \cos \Theta f_{IR}(-L) \right]^4 |d_{\vec{R},i}(-L)|^2$$

$$\times \left\{ 1 + 1 + 2 \cos \left(4 \omega_{IR} L + \Delta \phi^{xuv} + \Delta \varphi \right) \right\}$$

$\phi_{j^+}^{xuv} - \phi_{j^-}^{xuv}$

$\varphi_{j^+}(-L) - \varphi_{j^-}(-L)$

$$4 \cos^2 \left(2 \omega_{IR} L + \frac{1}{2} \Delta \phi^{xuv} + \frac{1}{2} \Delta \varphi \right)$$

low u SB : $n^- = 3, n^+ = -1$

$$P^{(c)}(\vec{R}, L) = E_{xuv}^2 |d_{\vec{R},i}(-L)|^2 \times$$

$$\times \left\{ \frac{1}{48^2} B_{IR}(\Theta, L)^6 + \frac{1}{4} B_{IR}(\Theta, L)^2 \right.$$

$$\left. + \frac{1}{48} B_{IR}(\Theta, L)^4 \cos \left(4 \omega_{IR} L + \Delta \phi^{xuv} + \Delta \varphi \right) \right\}$$

where

$$B_{IR} := E_{IR,0} \cos \Theta f_{IR}(-L)$$

Dipole M.E for $|L\rangle = |1s\rangle$

$$\begin{aligned}
d_{\vec{R}, 1s}^{\rightarrow}(\pm) &= (2\pi)^{-3/2} i \frac{d}{dP_z(\pm)} \int d^3r e^{-i\vec{p}(\pm)\cdot\vec{r}} \psi_{1s}(\vec{r}) \\
&= i \frac{d}{dP_z(\pm)} \psi_{1s}^{\rightarrow}(P(\pm)) \\
&= i \frac{8\sqrt{2}}{\pi} Z_i^{5/2} \frac{P(\pm)}{(Z_i^2 + P(\pm)^2)^3}
\end{aligned}$$

where $P(\pm) = |\vec{R} + \vec{A}_{IR}(\pm)|^2$
 $= R^2 + A_{IR}(\pm)^2 + 2\vec{R}\cdot\vec{A}_{IR}(\pm) \cos\Theta$

Comments

- for weak IR fields $d_{\vec{R}, L}^{\rightarrow}(\pm)$ depends weakly on Θ
- approximating $d_{\vec{R}, L}^{\rightarrow}(\pm) \approx |d_{\vec{R}, L}^{\rightarrow}(\pm)| e^{i\Theta} \hat{e}_j$ neglects the Θ dependence in $|d_{\vec{R}, L}^{\rightarrow}(\pm)|$. This assumes a weak ω_{XUV} dependence of the XUV photoionization cross section.
- in the exact $P(\vec{R}, L)$ on p.57 the XUV and IR temporal profiles are integrated over, as is the dipole M.E. This suggests the Θ dependence is dominated by the Volkov term (2. line), brought in by the absorption & emission of IR photons.